Phase transitions in Mn(Mo1–xWx)O4 oxides under the effect of high pressure and temperature

Veronica Blanco-Gutierrez, Alain Demourgues, Eric Lebraud, Manuel Gaudon

Phase transitions in $Mn(Mo_{1-x}W_x)O_4$ oxides under the effect of high pressure and temperature

Veronica Blanco-Gutierrez, Alain Demourgues, Eric Lebraud, and Manuel Gaudon*

Université de Bordeaux, CNRS, ICMCB, 87 Avenue du Dr. Albert Schweitzer, 33608 Pessac Cedex, France

Keywords $MnMoO_4$, phase transitions, pressure, sensors, temperature, tungsten, wolframite, X ray diffraction

*Corresponding author: e mail gaudon@icmcb bordeaux.cnrs.fr, Phone: +33 (0)5 40 00 66 85, Fax: +33 (0)5 40 00 27 61

ABO_4 compounds exhibit various phase transitions identified in the literature. The phase transitions between monoclinic α $C_{2/m}$ and wolframite $P_{2/c}$ structures of $Mn(Mo_{1-x}W_x)O_4$ compounds, which can be induced by pressure or temperature, are studied on the basis of X ray diffraction analyses. The large optical contrast associated with both these structures and Mo/W environments can be exploited to propose efficient piezochromic sensors (thanks to the monoclinic to wolframite transition vs. pressure) and thermal sensors (thanks to the reverse transformation), the thermochromic temperature being able to be tuned via the Mo/W ratio.

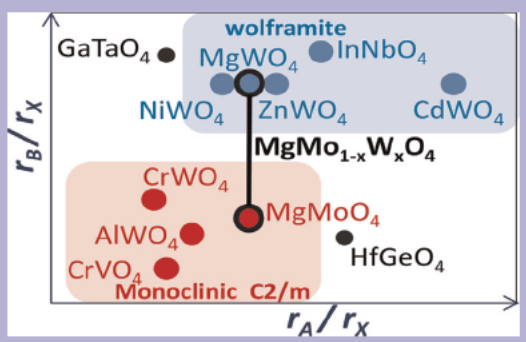

A(Mo,W)O_4 phase diagram: from wolframite to monoclinic compounds (drawn from the updated Bastide's diagram from Errandonea and Manjo [9]).

1 Introduction The phase transition between two allotropic forms can be exploited in a smart way to obtain sensors or actuators (especially to obtain thermal or strain sensors) [1 4]. As an illustration, our team has focused for many years on the $CuMoO_4$ and $CoMoO_4$ phase transitions for thermochromic or piezochromic properties [5 8]. More extensively, the ABX_4 compounds exhibit numerous crystalline forms and the phase transitions between some of them were shown to be of great interest [9]. The scheelite → fergusonite [10 12], wolframite → β-fergusonite [13 15], or zircon → scheelite [16 18] phase transformations were as illustration largely studied. In this paper, we concentrate on the $Mn(Mo_{1-x}W_x)O_4$ compounds; the two extreme compositions are, respectively, with monoclinic $C_{2/m}$ and wolframite structure. In the literature [19], it is known that molybdates with the monoclinic α-$MnMoO_4$ structure crystallize in the wolframite structure when synthesized at very high pressures. Therefore, in this present paper, we prepared a series of $Mn(Mo_{1-x}W_x)O_4$ compounds able to transform from the monoclinic allotropic form to the wolframite one while they are subjected to pressure. As-obtained wolframite stability versus temperature was finally investigated by *in situ* X-ray diffraction. The pressure-induced phase transition or reverse temperature-induced phase transition exhibited by a single compound make it suitable as a shock detector and a thermal sensor.

2 Experimental

2.1 Synthesis methods Samples of $MnMo_{1-x}W_xO_4$ with x: 0, 0.05, 0.1, 0.15, 0.2, 0.3, 0.4, and 1, named as 0, 05, 1, 15, 2, 3, 4, and W, respectively, were prepared by the solid-state route employing stoichiometric amounts of $MnCl_2 \cdot 4\,H_2O$ (Alfa Aesar, ≥99%), MoO_3 (Sigma Aldrich, ≥99.5%), and WO_3 (Alfa Aesar 99.8%) as reactants. After

homogenization of the reactants mixture by grinding in an agate mortar, the powder was placed in an alumina crucible and was thermally treated in air at 400 °C for 10 h with a 1 °C min ^{1} heating rate. The obtained powder was then homogenized by grinding in an agate mortar and treated at 500 °C for 10 h with a 1 °C min ^{1} heating rate. Low heating rates were needed in these two steps in order to obtain the monoclinic $C_{2/m}$ structure with no traces of sublimatable MoO_3. The samples were then treated at 1000 °C for 24 h with a 1 °C min ^{1} heating rate, in a sealed platinum tube containing Ar to avoid manganese oxidation. After each thermal treatment, the product was cooled down with a 2 °C min ^{1} rate. In order to induce the monoclinic to the wolframite phase transformation, the powder was mechanically treated by ball milling in an agate container half-filled with agate balls for 20 min in a 8000M/Mixer Mill SPEX apparatus.

2.2 Characterization techniques The structural characterization of the samples was performed by X-ray diffraction employing a Philips PW 1820 apparatus, with the Bragg Bentano geometry, equipped with a $K\alpha_1/K\alpha_2$ source and a copper anticathode. Diffraction patterns were collected with a 2θ step of 0.02° between 20 and 45° with a counting rate of 10 s per step in the routine mode. The structures were refined by the Rietveld method using Fullprof software. For the *in situ* high-temperature characterizations, the experiments were made on a PANalytical X'pert, equipped with a back monochromator ($K\alpha = 1.5418$ Å) and an Argon-Paar HTK16 chamber. The same heating thermal sequence (the temperature steps for diffractogram recording are fixed at 25, 100, 200, 300, 350, 400, 450, 500, 550, and 600 °C) was used for the two compared powders.

Diffuse reflectance spectra $R_{(\lambda)}$ were recorded at room temperature using a Cary 17 spectrophotometer with an integration sphere in the 350 850 nm wavelength range and a 1-nm step and a 2-nm bandwidth. Halon (PTFE: polytetrafluoroethyene) was used as a white reference. The spectra were used to obtain the La^*b^* space colorimetric parameters (L, luminosity; a^*, the green to red axis; and b^*, yellow to blue axis coefficients). The spectra were plotted in Kubelka Munk transform coordinates (K/S), with $K/S = (1 - R_{(\lambda)}{}^2)/(2R_{(\lambda)})$ versus photon energy.

3 Results

3.1 $MnMoO_4$–$MnWO_4$ binary phase diagram The binary phase diagram defined considering the two extreme $MnMoO_4$ $MnWO_4$ compositions, with respectively α-monoclinic and wolframite crystallographic forms (Fig. 1), was obtained from X-ray diffraction analysis of the various intermediate compositions. This diagram exhibits two solid solutions separated by a large biphasic domain. To build the diagram, the Rietveld refinements of the pattern of all the samples were used: both the cell parameters and the phase percentages when the latter are available (i.e., in the biphasic domain), are exploited.

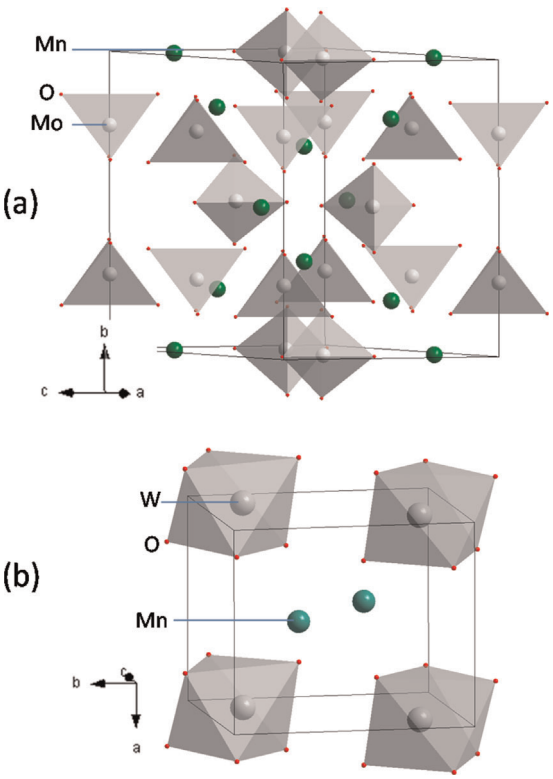

Figure 1 (a) $MnMoO_4$ α monoclinic structure (ICSD 248759) and (b) $MnWO_4$ wolframite structure (ICSD 78328).

The Rietveld refinements are illustrated in the three observed typical cases: in the monoclinic solid solution domain for the Mn-rich compositions, in the wolframite solid solution domain for the W-rich compositions, and in the biphasic domain for intermediate compositions (Fig. 2). The unit-cell parameters and the two phase concentrations are extracted with also the R_p and R_{wp} factors. In this way, the atomic positions were kept fixed on the ones proposed, respectively, in the ICSD-248759 and ICSD-78328 for monoclinic and wolframite phases, with isotropic displacement factors fixed to 0.5 Å^2 for cations and 1.0 Å^2 for oxygens. The most straightforward discrepancy index [20], the weighted profile R-factor R_{wp}, is about 6 7% in the solid solution domain and about 8 9% in the biphasic domain, what shows a good refinement quality. The a, b, c, and β cell parameters corresponding to the monoclinic form were plotted versus the tungsten composition (see Fig. 3). All the plots show a linear increase of the cell parameters versus the tungsten concentration until their stabilization for a composition near 17 mol% of tungsten. This linear increment is correlated to the larger ionic radius of tungsten (4d transition metal) in comparison with the molybdenum (3d transition metal). The stabilization of these parameters indicates the solubility limit (the maximal substitution of the molybdenum for the tungsten) is reached. This solid solution limit is confirmed by the plot of the monoclinic and tungsten fraction versus the tungsten composition (see Fig. 3, bottom part). The biphasic domain extracted

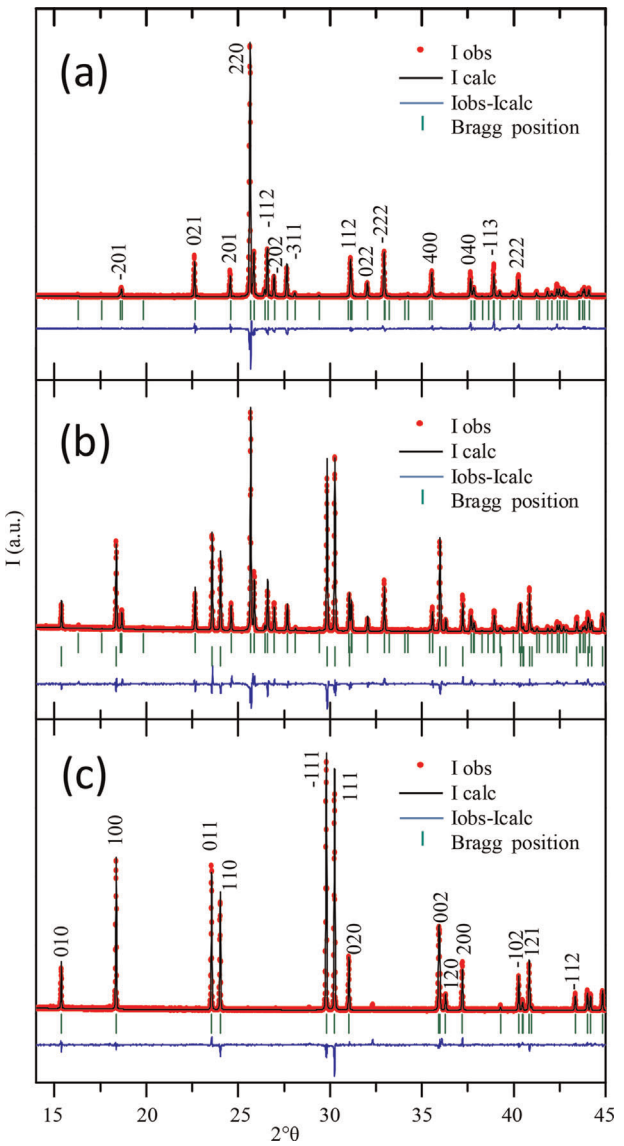

Figure 2 Rietveld refinement illustrations (experimental, calcu lated, and difference spectra) on the $Mn(Mo_{1-x}W_x)O_4$ samples with (a) $x = 0$; (b) $x = 0.4$; and (c) $x = 1$.

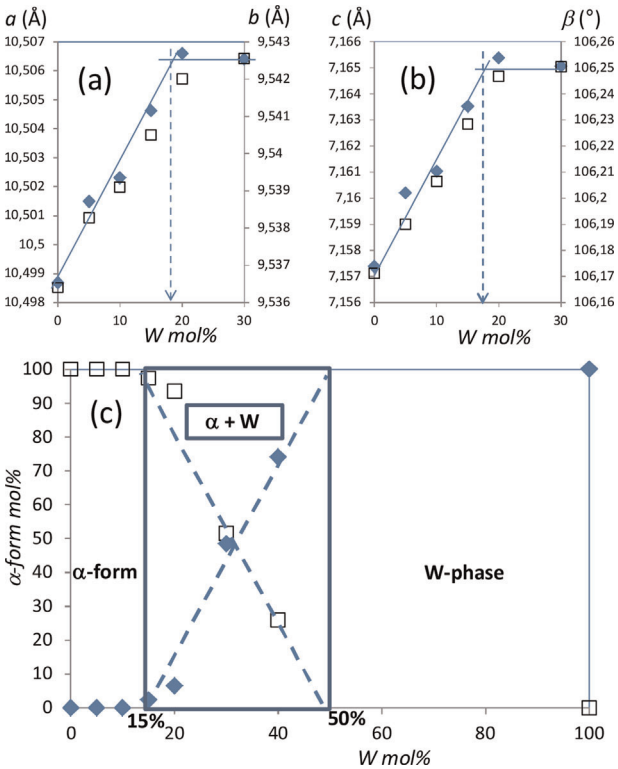

Figure 3 (a,b) Unit cell parameters evolution and concentra tion of the monoclinic and/or wolframite forms versus x in $Mn(Mo_{1-x}W_x)O_4$. (c) Binary phase diagram deduced directly from the α form (monoclinic form) content for various tungsten concentrations.

from this analysis was shown to range from about 15 to 50 mol% of tungsten.

The wolframite solid solution domain is a wide domain, i.e., the maximal substitution of the tungsten for the molybdenum is near 50%.

3.2 Chromic properties It can be noted that as far as we know, the $MnMoO_4$ and $MnWO_4$ were already studied for their photoluminescence (PL) properties but not for their chromic properties [21, 22]. The optical properties have been studied from 0.5 to 6 eV for the 0, 2, and W samples (see Fig. 4a). All the samples have a direct semi-conductor characteristic with at least one main charge transfer band (gap) corresponding to the O → Mo (or O → W, depending on the composition) and a Gaussian absorption band centered at about 2.2 2.3 eV which corresponds to d d intraelectronic transfer. From the Tanabe Sugano diagram [23] and the numerous studies on the coloration associated with the manganese II cation, the d d absorption band can be clearly indexed as the $^6A_1 \rightarrow {}^4T_1$ transition.

This band is spin forbidden ($\Delta S \neq 0$) and by the Laporte rule ($\Delta L = 0$) as well, since the octahedral site is centrosymmetric. Thus, the Gaussian absorption band exhibits a low intensity. From the numerous studies found on $AMoO_4$ molybdates, it can be clearly asserted that the O → W main gap occurred at lower energy than the O → Mo gap because of the higher iconicity of the O W bonds in comparison with the O Mo one. This comparison can be done only if the two cations have the same coordination number. Indeed, for the same M O bond, the gap associated with octahedral sites in these compounds, was located at lower energy than the gap associated with tetrahedral sites; the splitting between bonding and nonbonding molecular orbitals is increased by the orbitals recovering and it is higher for short tetrahedral bonds than for long octahedral ones. These considerations well explain the large energy difference between the gap position observed for $MnWO_4$ (about 2.5 eV) and $MnMoO_4$ (about 3 eV), in which the W and Mo ions are, respectively, in octahedral and tetrahedral sites. In the case of the monoclinic compound

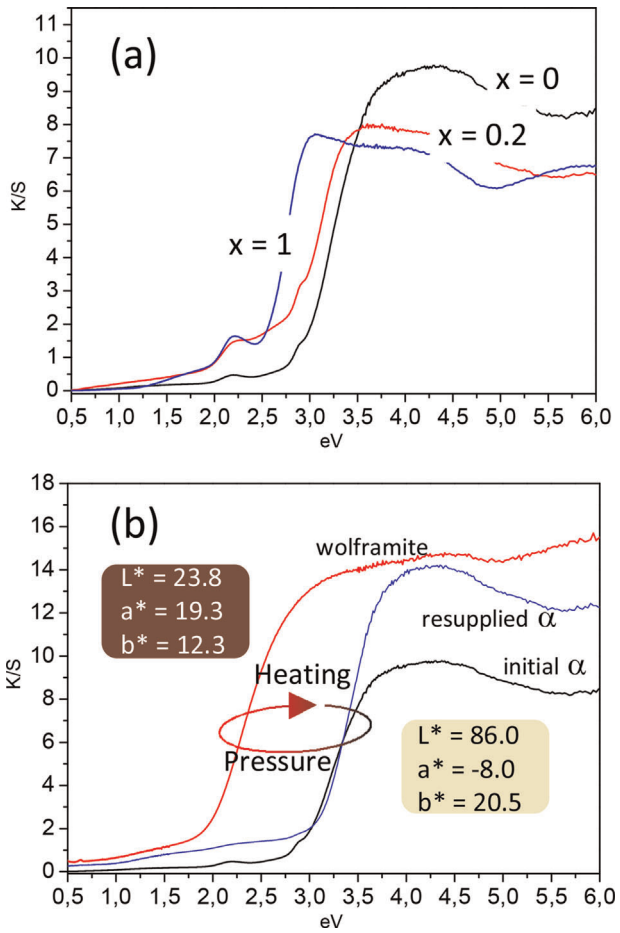

Figure 4 *K/S* absorption spectra of (a) $Mn(Mo_{1-x}W_x)O_4$ samples with $x = 0$; $x = 0.2$; and $x = 1$ and (b) for the $MnMoO_4$ samples: as synthesized, transformed by grinding into wolframite form and retransformed into monoclinic phase by thermal treatment.

with $MnMo_{0.8}W_{0.2}O_4$ formulae, the gap situation (2.7 eV) is intermediate.

3.3 Phase transitions The piezochromic/thermochromic properties associated, respectively, to the transformation from the monoclinic solid solution compounds to wolframite phase under pressure and to the opposite transformation versus temperature from wolframite phase to the monoclinic form have been investigated. The synthesized monoclinic phases, with compositions ranging from $MnMoO_4$ to $Mn(Mo_{0.8}W_{0.2})O_4$, nearly fully transform into wolframite phase with pressure, although some traces of residual monoclinic form can nevertheless be detected. The actual pressure transferred by the shock of the agate balls during ball milling is rather difficult to evaluate. From previous experiments on $Sr_{1-x}Ca_xCO_3$ vaterite to calcite transformations achieved with the same apparatus, it was already estimated that the ball-milling process allows phase transformation that have equivalent isostatic transition pressures reported in the literature in the range 1–10 GPa [24, 25].

SEM investigations on sample 15: as-synthesized with monoclinic form (Fig. 5a) and after mechanical grinding to induce the monoclinic to wolframite transformation (Fig. 5b) are reported for morphological comparison. SEM investigations are not adequate to confirm or otherwise the presence of deleterious phase, but interestingly, the impact of the mechanical treatment for the piezochromic transition on the crystallite morphology is well evidenced: the as-synthesized compound exhibits large isotropic crystallites with a rounded surface, while the ball-milled compound exhibits more angular crystallites.

The thermal evolutions of the metastable wolframite obtained after mechanical grinding of the undoped and the 15 mol% W-doped compounds were compared by X-ray diffraction analyses (see Fig. 6; here, respectively, the traces of wolframite and monoclinic phases are marked with asterisks). As can be seen, the 600 °C treatment on the obtained wolframite phase has a different effect depending on the composition. For the undoped compound, the "retransformation" from wolframite to monoclinic phase is observed between 400 °C and 500 °C, whereas the wolframite phase remains unchanged for sample 15 up to 600 °C. Nevertheless, an annealing treatment of the latter sample at 750 °C for 10 h, produces the retransformation to the monoclinic structure. Hence, these studies show that

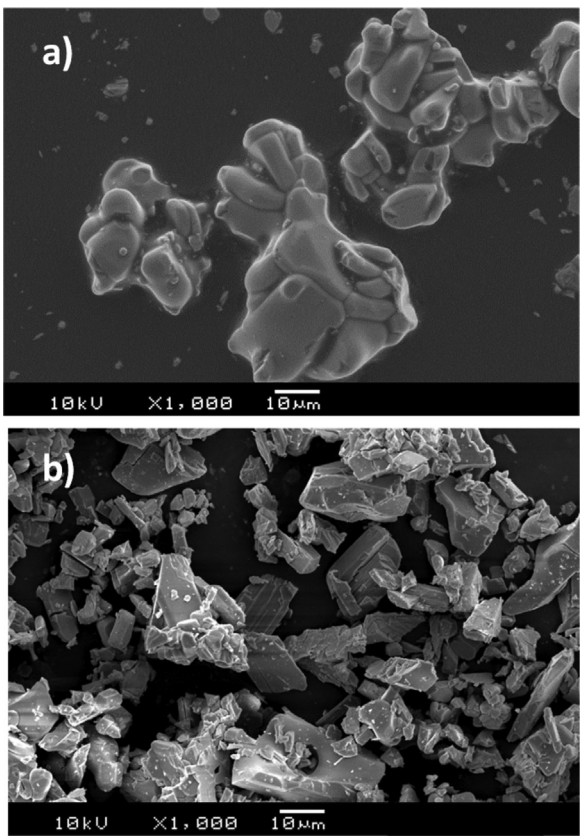

Figure 5 SEM images of $Mn(Mo_{0.85}W_{0.15})O_4$ sample: (a) as synthesized with monoclinic form, (b) transformed by grinding into wolframite form.

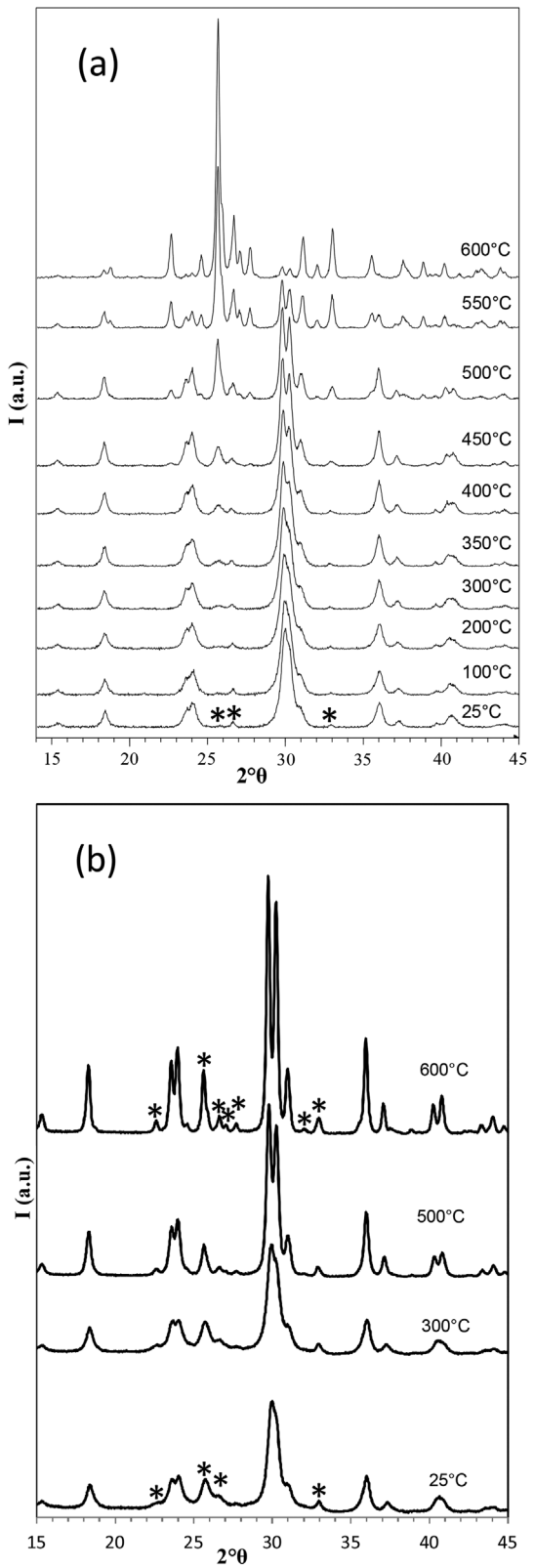

Figure 6 Comparison of the *in situ* X ray diffraction analyses versus thermal treatment temperature made on the $MnMoO_4$ wolframite compound (a) and the $Mn(Mo_{0.85}W_{0.15})O_4$ wolframite compound (b).

monoclinic $Mn(Mo_{1-x}W_x)O_4$ compounds are able to transform under high pressure (induced through an efficient mechanical miller) to a metastable wolframite phase, while the latter can be used as a thermal sensor since the retransformation to the monoclinic phase can be activated by a thermal treatment. Furthermore, the quantity of tungsten has an important influence on the temperature of the retransformation from wolframite to monoclinic phase versus temperature. Indeed, the strong preference of the W^{6+} ions for octahedral sites (as in wolframite phase) in comparison with the Mo^{6+} ions that exhibit a strong tetrahedral site preference (as in the monoclinic form), induces an energetic stabilization of the wolframite form and so an increase of the retransformation temperatures as the tungsten content increases. The optical contrast between the metastable wolframite and the initial monoclinic form (before grinding) or the final monoclinic form (after thermal treatment of retransformation) is illustrated in Fig. 4b for the $MnMoO_4$ compound.

The optical contrast between the two monoclinic forms is negligible. On the contrary, the coloration of the wolframite form is significantly different (darker) in comparison with the monoclinic samples. Indeed, a large charge-transfer band displacement from the UV region (3 eV) to the visible (1.9 eV), associated with the change of coordination of the Mo^{6+} ions from 4 to 6 is seen when going from the monoclinic samples to the wolframite one.

4 Conclusions Efficient thermochromic thermal sensors with the possibility to tune the marked temperature can be obtained. In our example, Mo-rich $Mn(Mo_{1-x}W_x)O_4$ metastable wolframite forms, obtained by a mechanical alloying of $Mn(Mo_{1-x}W_x)O_4$ monoclinic phases, are associated with a retransformation to the monoclinic stable form versus temperature. The retransformation is associated with a drastic thermochromic behavior and the marked temperature can be tuned with the tungsten concentration. Hence, the study opens up the window for the use and the optimization of a new generation of shock sensors and thermal sensors.

Acknowledgement The authors are thankful to L'Agence Nationale de la Recherche for financial support under the ChoCoComp project (ANR 13 RMNP 0011).

References

[1] H. Eilers, R. Gunawidjaja, T. Myint, J. Lightstone, and J. Carney, AIP Conf. Proc. **1426**, 1577 1580 (2012).
[2] B. Hu, Y. Ding, W. Chen, H. Kulkarni, Y. Shen, V. V. Tsukruk, and Z. L. Wang, Adv. Mater. **22**, 5134 5139 (2010).
[3] L. A. Bashkirov, N. Y. Shishkin, O. I. Kurbachev, O. A. Chebotar, and I. M. Zharsky, Sens. Actuators B **55**, 65 69 (1999).
[4] A. Rabhiou, J. Feist, A. Kempf, S. Skinner, and A. Heyes, Sens. Actuators A **169**, 18 26 (2011).

[5] M. Gaudon, P. Deniard, A. Demourgues, A. E. Thiry, C. Carbonera, A. Le Nestour, A. Largeteau, J. F. Létard, and S. Jobic, Adv. Mater. **19**, 3517 3519 (2007);
M. Gaudon, A. E. Thiry, A. Largeteau, P. Deniard, S. Jobic, J. Majimel, and A. Demourgues, Inorg. Chem. **47**, 2404 2410 (2008);
M. Gaudon, C. Carbonera, A. E. Thiry, A. Demourgues, P. Deniard, C. Payen, J. F. Letard, and S. Jobic, Inorg. Chem. **46**, 10200 10207 (2007);
V. Blanco Gutierrez, A. Demourgues, and M. Gaudon, Dalton Trans. **42**, 13622 13627 (2013).

[6] E. L. S. Souza, C. J. Dalmaschio, M. G. R. Filho, G. E. Luz Jr, R. S. Santos, E. Longo, and L. S. Cavalcante, Microscopy: Advances in Scientific Research and Education (Formatex Research Center, Badajoz, Spain, 2014).

[7] J. Ruiz Fuertes, A. Friedrich, J. Pellicer Porres, D. Errandonea, A. Segura, W. Morgenroth, E. Haussühl, C. Y. Tu, and A. Polian, Chem. Mater. **23**, 4220 4226 (2011).

[8] R. Lacomba Perales, J. Ruiz Fuertes, D. Errandonea, D. Martínez García, and A. Segura, Europhys. Lett. **83**, 37002 (2008).

[9] D. Errandonea and F. J. Manjo, Prog. Mater. Sci. **53**, 711 773 (2008).

[10] V. Panchal N. Garg, A. K. Chauhan, B. Sangeeta, and S. M. Sharma, Solid State Commun. **130**, 203 (2004).

[11] A. Grzechnik, W. A. Crichton, M. Hanfland, and S. Van Smaalen, J. Phys.: Condens. Matter **15**, 7261 (2003).

[12] A. Grzechnik, W. A. Crichton, and M. Hanfland, Phys. Status Solidi B **242**, 2795 (2005).

[13] F. J. Manjón, D. Errandonea, J. López Solano, P. Rodríguez Hernández, S. Radescu, A. Mujica, A. Muñoz, N. Garro, J. Pellicer Porres, A. Segura, Ch. Ferrer Roca, R. S. Kumar, O. Tschauner, and G. Aquilanti, Phys. Rev. B **73**, 224103 (2006).

[14] A. Perakis, E. Sarantopoulou, and C. Raptis, High Press. Res. **18**, 181 (2000).

[15] W. J. Sun, F. J. Ma, and S. J. Zhuang, Sci. Geol. Sinica **1**, 78 (1983).

[16] A. Jayaraman, G. A. Kourouklis, G. P. Espinosa, A. S. Cooper, and L. G. V. Uitert, J. Phys. Chem. Solids **48**, 755 (1987).

[17] X. Wang, I. Loa, K. Syassen, M. Hanfland, and B. Ferrand, Phys. Rev. B **70**, 064109 (2004).

[18] F. J. Manjon, S. Jandl, G. Riou, B. Ferrand, and K. Syassen, Phys. Rev. B **69**, 165121 (2004).

[19] R. O. Keeling Jr, Acta Crystallogr. **10**, 209 (1967).

[20] B. H. Toby, Powder Diffr. **21**, 67 70 (2005).

[21] H. Kähäri, J. Juuti, S. Myllymäki, and H. Jantunen, Mater. Res. Bull. **48**, 2403 2405 (2013).

[22] M. A. P. Almeida, L. S. Cavalcante, J. A. Varela, M. Siu Li, and E. Longo, Adv. Powder Technol. **23**, 124 128 (2012).

[23] Y. Tanabe and S. Sugano, J. Phys. Soc. Jpn. **9**, 753 766 (1954); J. Phys. Soc. Jpn. **9**, 766 779 (1954); J. Phys. Soc. Jpn. **11**, 964 977 (1956).

[24] M. A. P. Almeida, L. S. Cavalcante, M. Siu Li, J. A. Varela, and E. Longo, J. Inorg. Organomet. Polym. 22, 264 271 (2012).

[25] V. Blanco Gutierrez, A. Demourgues, V. Jubera, and M. Gaudon, J. Mater. Chem. C **2**, 9969 9977 (2014).